Electrical characterization of inkjet printed conductive traces using LinuxCNC

Christoph Beisteiner, Robert Wallner and Bernhard G. Zagar
Johannes Kepler University Linz
Institute for Measurement Technology
Altenberger Straße 69, 4040 Linz, Austria
E-mail: christoph.beisteiner@jku.at, robert.wallner@jku.at and bernhard.zagar@jku.at

***Abstract*—This paper presents a method of measurement to characterize the quality of inkjet printed conductive traces created with a commercially available desktop printer. Its focus lies on the investigation of the electrical connectivity and the current density distribution within a trace, as these are the main indicators for the usability of printed conductive traces. Usually electrical circuit boards (PCBs) contain arbitrary plain geometries, but due to the flexibility of the substrate on which the traces are printed a 3D scanning measuring system is needed, this allows the traversing of all axes simultaneously which usually is not implemented in state-of-the-art measurement systems. To overcome this constraint the open-source project LinuxCNC was selected as a numerical control system to scan geometries, such as helical traces (e.g., coils), by using linear and circular movements. By combining this measurement system with a giant magnetoresistance sensor (GMR) and a four-point probe measurement method, rapid characterization of the quality of inkjet printed traces was possible.**

I. Introduction

Inkjet printed conductive traces play an increasingly important role in product design and rapid prototyping PCBs. Usually, conductive printed traces are fabricated by screen printing technology, but nowadays it is possible to print conductive inks with any commercially available desktop printer. Traces can be printed on any kind of substrates such as paper, synthetic material, or textiles just to name a few. Advantages lie in production cost, simplicity of manufacture and printing on recyclable paper. Designing passive components of electrical circuits like resistors, capacitors (up to $50\,\mathrm{pF}$ [1]), or inductors (spiral inductors with an inductance up to $25\,\mathrm{nH}$ were shown in [2]) is possible. This innovative technique enables designing of complete electrical circuits. Even printing sensors like strain gauges is feasible. Nevertheless, designing multilayer circuits and soldering of components are future challenges.

In the field of electrical engineering, the application area ranges from wearable flexible capacitors to inductive position sensors [1], [3]. Another application is the usage of low cost, printed antennas for RFID applications on flexible materials [4]. A further scope of application is to use conductive printed ink on a transparent substrate as optical photo mask, due to the increased optical density compared to standard ink, due to the presence of metallic nanoparticles.

Limiting factors of printed traces are long term stability and the heat, or the scratch resistance. These quality parameters can be analyzed with different measurement methods like

- ultrasound transit runtime measurement
- image acquisition with a CCD-chip (e.g., digital camera),
- spatially measuring the temperature,
- measuring electric potential differences,
- and magnetic fields.

Measuring the magnetic field and measuring an electrical potential difference across a printed trace are used as preferred analyzing techniques in this paper.

II. Adaptable measurement system

LinuxCNC is a powerful open-source motion control software with a project architecture that is adjustable for individual purposes [5]. The hardware structure of the realized measurement system is shown in Fig. 1. The main component is a x86 PC with a LinuxCNC Ubuntu 10.04 distribution [6]. In this system a Linux kernel with a Real Time Application Interface (RTAI) was installed for compiling LinuxCNC and the Control and Measurement Device Interface (COMEDI) [7]. COMEDI is used to read measurement data from a data acquisition card (DAQ) like a NI-6221 card. This is suitable for acquiring data from different sensors with an electrical output signal. LinuxCNC is applied to traverse all axes of a gantry robot simultaneously, and thus it is possible to scan arbitrary geometries (with circular movements, or helical movements). E.g. scanning of antennas on three dimensional (3D) surfaces is possible [8]. Furthermore scanning of printed 3D electronics or capacitive sensors can be done.

A. LinuxCNC extensions

LinuxCNC supports building extensions with modules, which are able to share data with the software library of the hardware abstraction layer (HAL) in real time. An overview of the software implementation with already existing and newly developed modules is shown in Fig. 2. The data exchange between each module is performed by the HAL. The module `emcrsh.cc` receives commands by using TCP/IP to control the G-code interpreter. `hal_paraport.c` provides the motor control signals calculated by the path control unit to the hardware. The module `hal_comedidri.c` was developed for transferring data from the COMEDI to the HAL. It reads and writes data with the COMEDILib from the NI PCI-6221 DAQ card in real time. The developed data logger module `logger_rt.c` stores the measured values and the absolute positions, generated by the path control unit, into a circular

978-1-4799-6144-6/15/$31.00 ©2015 IEEE

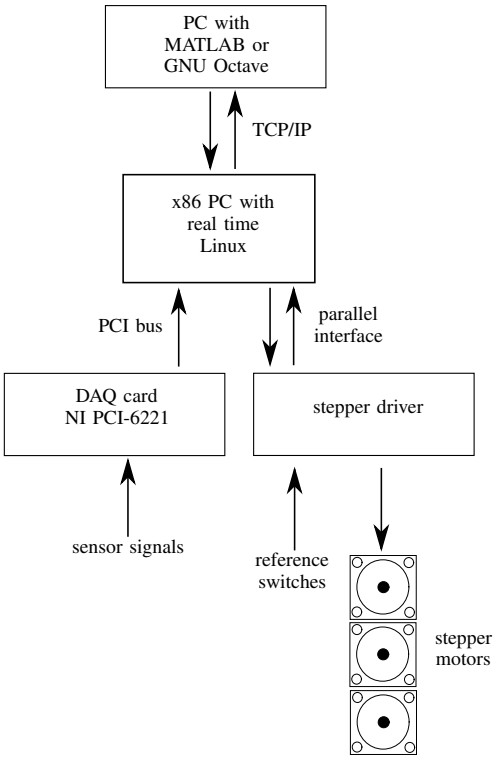

Fig. 1. Concept of the interaction between the components of the measurement system.

buffer. The user space part of the data logger `logger.c` provides the stored content by using a TCP/IP server to a client software like MATLAB or GNU Octave. For system performance reasons the circular buffer has a fixed size of 2000 entries, where each entry has space for 8 channels. With a cycle time of 1 ms, up to 2 seconds of data can be buffered. Within this time frame the client software has to request and process the data, otherwise samples will be lost. One way to prevent this loss is a built-in adjustable clock divider to reduce the sampling rate which reduces the amount of data.

B. Control system details

The movement of each axis is directly operated over a step-direction interface through the parallel port of the x86 system to the hardware. The developed hardware uses three TMC262 stepper drivers to control all kinds of gantry robots, which are using stepper motors with peak currents of up to 7 A per motor. Due to a risk of collision the TMC262 driver provides a stall guard detection which warns if the mechanical load on the stepper motor is too great. This can be useful for time intensive measurements to prevent the setup from being damaged.

C. Software and hardware limits

The maximum scanning velocity is a compromise between the maximum spatial resolution and the minimal base period of the real time system. With the minimal base period t_{Base}, the adjusted microsteps μ_{Steps}, the motor steps m_{Steps} and the

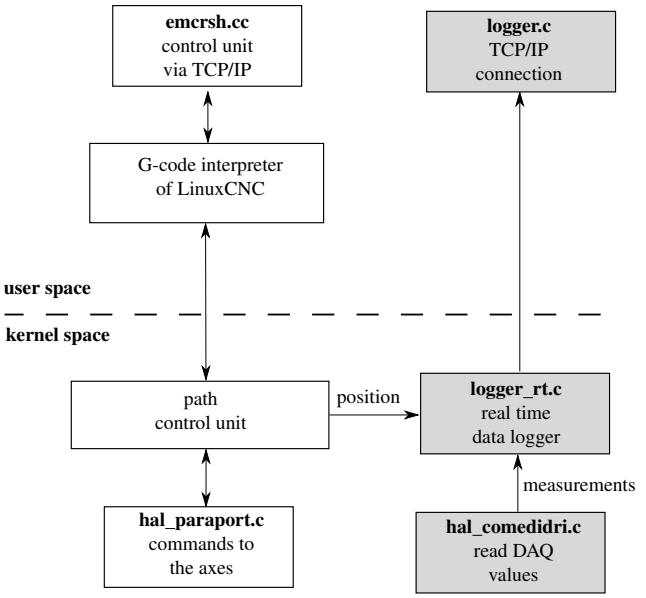

Fig. 2. Principle of the data exchange between the LinuxCNC modules using the HAL. All newly developed components are shaded.

screw pitch p, the velocity

$$v_{\text{max}} = \frac{p}{m_{\text{Steps}} \cdot \mu_{\text{Steps}} \cdot t_{\text{Base}}} \tag{1}$$

and the spatial resolution

$$x_{\text{res}} = \frac{p}{m_{\text{Steps}} \cdot \mu_{\text{Steps}}} \tag{2}$$

can be calculated. The control PC used allows for a minimal base period of $55\,\mu\text{s}$, which provides a step-dir signal with a frequency of $18.2\,\text{kHz}$. The gantry system, which was built with LINOS x.act axes, provided 200 steps/rev motors, a screw pitch of $2\,\text{mm/rev}$ and a scanning volume of $100\,\text{mm} \times 100\,\text{mm} \times 100\,\text{mm}$. With the selected 16 microsteps per full step, a maximum velocity of $11.4\,\text{mm/s}$ and a spatial resolution of $0.6\,\mu\text{m/step}$ are obtainable.

III. Measurements on inkjet printed traces

Different parameters like heat capacity, thermal and electrical conductivity, thermal stability and ink layer thickness are quality factors and therefore important to evaluate. These parameters depend on the ink and the substrate used. Ready-to-use inks are the Silver Nano-particle ink from Mitsubishi [9] or Silver Bullet ink from Xerox [10]. Substrates can be Canon Photo Plus Glossy II, HP Premium Plus Photo paper and Mitsubishi Nano Benefit NB-TP-3GU100 inkjet printable PET films.

Another influence factor is how the pressure to eject the ink from the nozzle is generated. This pressure pulse can be induced with a piezoelectric element or by heating (bubble jet) [11]. A Brother DCP-J552DW inkjet printer with a piezoelectric head was used, because of the lack of thermal influence onto the ink and the bigger nozzles which allow to print the Mitsubishi ink with a 20 nm nano-particle size. Due to the higher conductivity achieved, a Canon Photo Plus Glossy II with a resulting ink layer thickness of $2\,\mu\text{m}$ was used and measured by a Bruker Dektak XT profilometer.

Fig. 3. Test object to measure the electrical conductivity with increasing printed gray level on Canon Photo Plus Glossy II substrate. The gray level is varied from 100% (left) to 40% (right) with steps of 3%. Additionally the test object was baked at 60 °C for half an hour to increase the electrical conductivity. The reason for this to be effective is, that silver nano particles have a greatly reduced melting temperature compared to bulk silver [13].

The maximum continuous power dissipation was measured to be approximately $450\,\mathrm{mW/cm^2}$, by stepwise increasing the applied current until the printed conductive trace was destroyed. Due to the small heat capacity it can be assumed that the peak power dissipation (a pulse with a few microseconds) is roughly the same as the maximum continuous power dissipation, which can be explained via the heat transfer equation [12]:

$$A \cdot h \cdot c_p \cdot \dot{T} = \alpha \cdot A \cdot (T_u - T) + \dot{Q} \tag{3}$$

with the heat capacity of the silver nano particles and the substrate c_p, the heat transfer coefficient α, the ambient temperature T_u, the object temperature T, the printed inkjet area A and the layer thickness h. Due to the thin layer h the response time of the thermal system

$$\tau = \frac{h c_p}{\alpha} \tag{4}$$

is negligible. Accordingly, Eq. (3) reduces to the stationary solution

$$\dot{Q} = \alpha \cdot A \cdot (T - T_u). \tag{5}$$

That the peak power dissipation and the maximum continuous power dissipation are equal was finally proven by measurement.

A. Electrical conductivity measurement

It is assumed that varying in printed gray levels influences the electrical conductivity, because of changes in the distance between the cluster of nano particles. This could be used properly to design inkjet printed resistors. To determine the conductivity of a printed trace as a function of the printed gray level, a test problem with increasing gray levels was designed. A photo of the sheet is shown in Fig. 3.

The electrical conductivity is measured by a constant current excitation of $158\,\mathrm{mA}$ and measuring the spatial resolved potential difference U_y between two spring loaded contacts with a distance of $d_y = 2.5\,\mathrm{mm}$.

While probing over a rectangular grid with a circular boundary the electrical potential differences were amplified using an AD8421 instrumentation amplifier with a voltage gain of 1000. The analog voltages were provided to the DAQ card. Further smoothing of the measurements was performed in software by calculation of the mean value. The measurement method is shown in Fig. 4.

Due to the known layer thickness t, the width of a printed rectangular trace b and the current I through the measuring object, the conductivity σ can be obtained by

$$\sigma = R \cdot \frac{b \cdot h}{d_y} = \frac{U_y}{I} \cdot \frac{b \cdot h}{d_y}. \tag{6}$$

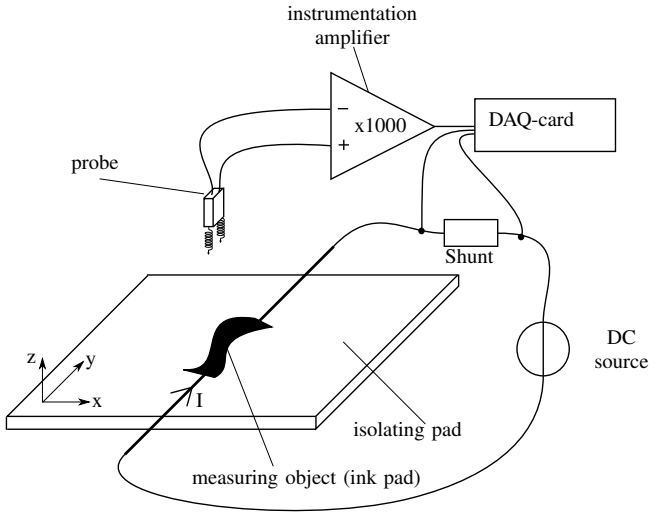

Fig. 4. Measurement principle based on using two probes with spring contacts.

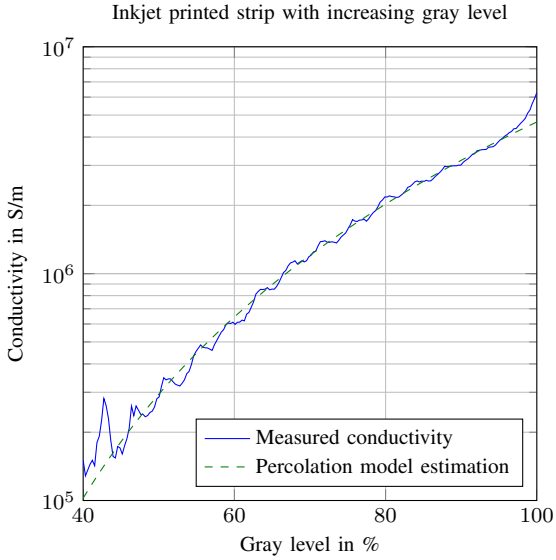

Fig. 5. Measured conductivities along a printed trace with an increasing gray level. The ripples are due to the discrete gray levels of the printed test object.

In Fig. 5 the conductivity over the gray level is shown.

Furthermore, based on these data the percolation model

$$\sigma(p) = \begin{cases} 0, & \text{if } p < p_c \\ \sigma_0 \cdot (p - p_c)^t, & \text{if } p \geq p_c \end{cases} \tag{7}$$

with a constant proportionality σ_0, percolation threshold p_c and the critical exponent t can be applied. Finally, the data has been fitted to $\sigma_0 = 7.82 \cdot 10^6\,\mathrm{S\,m^{-1}}$, $p_c = 15.4\%$ and $t = 3.09$ with a non-linear regression method which confirms the assumption of correlation between conductivity and gray level [14].

B. Current distribution via spring probing

To determine the homogeneity of the inkjet printed conductive traces the current density distribution within the specimen can be utilized. A circular conductive plane was printed for testing the proposed measurement method and, furthermore, to demonstrate the feasibility of the system to measure along

circular trajectories. Therefore, the current density does not only vary due to the homogeneity of the conductivity but also due to the circular shape of the conductor.

Based on the mathematical relationship

$$E_y(x,y) = \frac{U_y(x,y)}{d_y} \tag{8}$$

the electric field strength E_y provided to the spring contacts with a distance d_y can be calculated [15].

The current density

$$J_y(x,y) = \sigma \cdot E_y(x,y) \tag{9}$$

can be calculated with the previously measured electrical conductivity σ and the measured electric field E_y.

The measured current densities of a circular shaped conductor trace with and without an inner hole are shown in Figs. 7(a) and 9(a). At a resolution of 2 mm/pixel a measurement of the sample patch takes approximately 40 min. Circular movements where used for efficiency reasons.

Discrepancies in the current measure can be caused by the spring contacts. Misalignment after the spring contacts are closed causes an error in the current density. Furthermore positioning errors can occur due to the gantry robot which can be at least 1 µm. Due to the high impedance measurement surface contamination doesn't influence the measurement results. To estimate the current density the electrical conductivity has to be known. This value is calculated using the measured layer thickness and the measured voltage drop over a trace length, in which a constant current is flowing. The layer thickness can vary from 1.8 µm to 2.2 µm along a printed trace, which causes another uncertainty. The trace length is a mechanic quantity with an uncertainty of 20 µm.

C. Current distribution via magnetic field measurement

Another way to generate an image of the current distribution is to measure the magnetic field spatially and solving the inverse problem [16]. Figure 6 shows the measurement principle to generate a measurable signal. The differential signal of the giant magnetoresistance (GMR) sensor (NVE AA005-02) is amplified by an instrumentation amplifier and a lock-in amplifier to generate an appropriate output signal. Because of the electromagnetic interference of the stepper drivers, caused by micro-stepping, the signal to noise ratio is low (−35 dB). These interferences are reduced by using a lock-in amplifier. An alternating current signal with a frequency of 457.12 Hz and an amplitude of 150 mA was used, with emphasis on not using a multiple of 50 Hz.

With the spatial lock-in amplifier output voltage $U_{\text{out}}(x,y)$ digitized by the DAQ-card, the sensitivity S, the bridge voltage U_v, the gain V_1 of the instrumentation amplifier and gain V_2 of the lock-in amplifier, the magnetic field

$$H(x,y) = \frac{U_{\text{out}}(x,y)}{U_v \cdot S \cdot V_1 \cdot V_2} \tag{10}$$

is calculated. For the measurement assembly a bridge voltage of $U_v = 24\,\text{V}$, a sensitivity of $S = 6.91\,(\mu\text{V/V})/(\text{A/m})$, and amplifier gains of $V_1 = 163$ and $V_2 = 40$ were used.

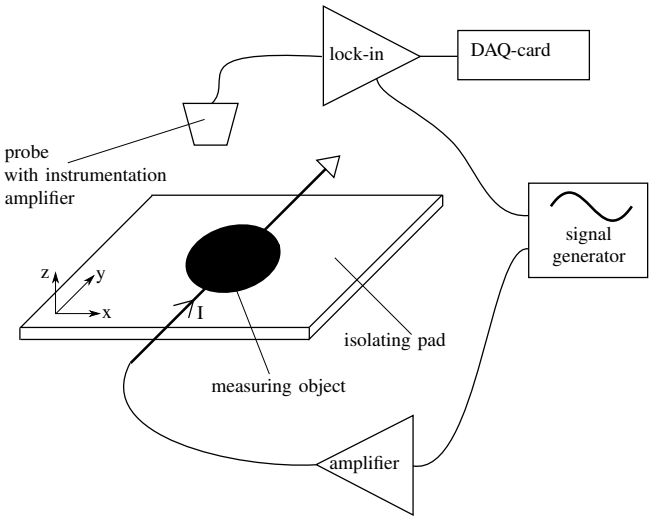

Fig. 6. Principal measurement assignment to use an GMR sensor with the presented measurement system

The relationship between the spatially resolved magnetic field strength $H_x(x,y)$ and the spatial current density $J_y(x,y)$ within a thin plane structure is given by the convolution

$$H_x(x,y) = J_y(x,y) * G_{\text{Biot}}(x,y) \tag{11}$$

with Green's filter function [17]

$$G_{\text{Biot}}(x,y,z) = \frac{zh}{4\pi \cdot (x^2+y^2+z^2)^{3/2}} \tag{12}$$

in the spatial domain and transformed to frequency domain with

$$G_{\text{Biot}}(u,v) = \mathcal{F}(G_{\text{Biot}}(x,y)) = \frac{h}{2} \cdot \exp\left(-2\pi \cdot z \cdot \sqrt{u^2+v^2}\right) \tag{13}$$

with a known distance z between sensor and measuring object, known layer thickness h and the corresponding frequency domain coordinates u and v. Furthermore, Eq. 11 is an inverse problem that was finally solved with the Richardson-Lucy deconvolution algorithm [18].

Another circular conductive plane with a missing hole in the center was printed to demonstrate issues of the spring measurement method. Due to the only one-sided contact of the probes in the boundary region of the centered hole, at least one input of the instrumentation amplifier is floating and therefore the measurement results are corrupted in this region. The estimated current densities of a circular shaped conductor with and without an inner hole are shown in Figs. 7(b) and 9(b). The measurement takes approximately 40 min for a spatial resolution of 0.1 mm/pixel, same time, 4 × resolution compared to previous method, as no spring loading is required.

D. Measurement results

In general, current density measurements with GMR sensors provide images with a higher spatial resolution (at same time consumption) as with spring probing. To detect even smallest faults within the conductive area, the spatial resolution of the utilized measurement method is an important parameter. For example the conductive ink of the test object in Fig. 8(a) has

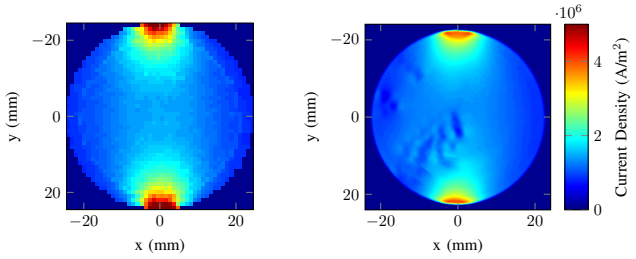

(a) Measured with spring contacts. (b) Measured with a GMR

Fig. 7. Current distribution $J_y(x, y)$ of a printed disc.

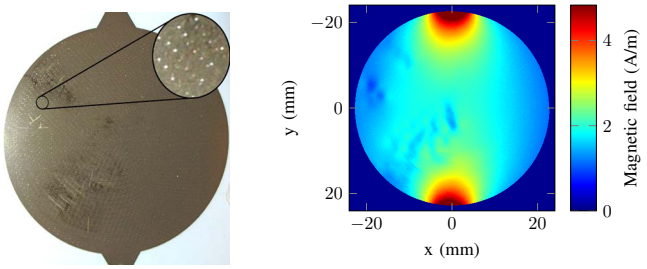

(a) Object under test. The detailed area shows the mechanical damage, due to the contact probes.

(b) Measured magnetic field

Fig. 8. Printed circle under test.

been removed by accidentally touching previously dried up surface. This shows how fragile the surface of the printed conductor on the Canon Photo Plus Glossy II paper is and how essential testing methods are for this technology. Furthermore, the picture also shows imprints of the probes of the spring probing setup.

The measurement results in Fig. 7(b) demonstrate the advantages of the magnetic field measurement method, since the local faults are clearly visible. Nevertheless, a much higher current amplitude is needed for this measurement method compared to the spring probing method, and this is an issue for test objects with small traces and structures. Additionally, it is necessary to determine the air gap between the test object and the sensor for solving the inverse problem. Therefore, the gap between the sensor and the object must be constant over the whole measuring area.

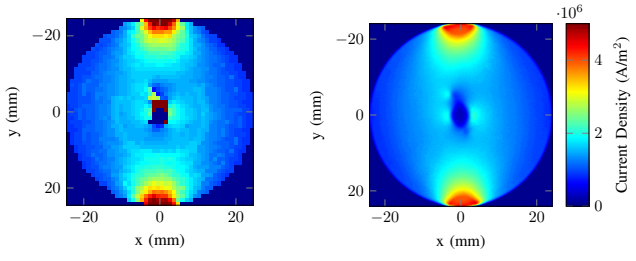

(a) Measured with spring contacts (b) Measured with a GMR

Fig. 9. Current distribution $J_y(x, y)$ of a printed disc with an inner hole.

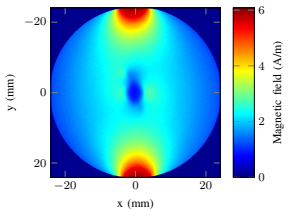

Fig. 10. Magnetic field of the printed circle with an inner hole.

The influence of a big artificial fault on an inkjet printed conductive trace was also tested. As test object a circle with a cut out hole was printed. The current density results are shown in Fig. 9(a) and Fig. 9(b). Measurement faults are visible in the inner hole (wrong high current densities) of the spring probing scan because of saturation effects caused by the instrumentation amplifier.

E. Alternative method

Local faults on a current-carrying printed trace are causing more power loss. This heat loss is a indicator for higher spatial temperatures and they can be measured with a temperature sensor or by infra-red thermography. Unfortunately a high enough spatial resolution and a high current is necessary to detect faults on the printed circuit.

IV. Conclusion

For investigation of inkjet printed traces, a measurement method to evaluate the printing quality was presented. Measurements included the current density and electrical connectivity of printed traces. With an adaptive measurement system it was possible to try different sensor concepts and to evaluate these parameters. LinuxCNC with an implemented COMEDI HAL module performed the task excellently.

Using the software tool, two different measurement principles were selected. With spring probing it was possible to measure the current density on a printed trace even with a very low feed current through the test object. The limited mechanical stability of a printed conductive trace was shown in this case. Furthermore, a contactless method with a GMR sensor was applied, too. The measurement results using the GMR deliver a higher spatial resolution compared with spring probing and are more effective in finding faults caused by bad printing.

Acknowledgment

The authors gratefully acknowledge the partial financial support for the work presented in this paper by Austrian Research Funding Association (FFG) under contact grant 843499 and WimTec Sanitärprodukte GmbH.

References

[1] Y. Li, R. Torah, S. Beeby, and J. Tudor, "An all-inkjet printed flexible capacitor for wearable applications," in *Design, Test, Integration and Packaging of MEMS/MOEMS (DTIP), 2012 Symposium on*, April 2012, pp. 192–195.

[2] B. Cook, C. Mariotti, J. Cooper, D. Revier, B. Tehrani, L. Aluigi, L. Roselli, and M. Tentzeris, "Inkjet-printed, vertically-integrated, high-performance inductors and transformers on flexible lcp substrate," in *Microwave Symposium (IMS), 2014 IEEE MTT-S International*, June 2014, pp. 1–4.

[3] N. Jeranče, D. Vasiljević, N. Samardžić, and G. Stojanović, "A compact inductive position sensor made by inkjet printing technology on a flexible substrate," *Sensors 2012, Basel*.

[4] A. Rida, L. Yang, R. Vyas, and M. Tentzeris, "Conductive inkjet-printed antennas on flexible low-cost paper-based substrates for rfid and wsn applications," *Antennas and Propagation Magazine, IEEE*, vol. 51, no. 3, pp. 13–23, June 2009.

[5] F. Tajti, G. Szayer, B. Kovacs, and P. Korondi, "Universal rt-middleware robot controller," in *Industrial Electronics Society, IECON 2013 - 39th Annual Conference of the IEEE*, Nov 2013, pp. 7862–7867.

[6] E. Siever, S. Figgins, R. Love, and A. Robbins, *Linux in a Nutshell*, ser. Nutshell. O'Reilly Media, 2009.

[7] D. Abbott, *Linux for Embedded and Real-time Applications*, ser. Embedded Technology. Elsevier Science, 2012.

[8] J. J. Adams, E. B. Duoss, T. F. Malkowski, M. J. Motala, B. Y. Ahn, R. G. Nuzzo, J. T. Bernhard, and J. A. Lewis, "Conformal printing of electrically small antennas on three-dimensional surfaces," *Advanced Materials*, vol. 23, no. 11, pp. 1335–1340, 2011. [Online]. Available: http://dx.doi.org/10.1002/adma.201003734

[9] Mitsubishi Imaging (MPM), Inc. (2013) Mitsubishi nanobenefit 3g series. 29-09-2014. [Online]. Available: http://www.mitsubishiimaging.com/digital-imaging-diamond-jet-NANOINK.html

[10] Xerox Corporation. (2014) Xerox scientists develop silver ink to print plastic circuits. 29-09-2014. [Online]. Available: http://www.xerox.com/innovation/news-stories/silverbullet/enus.html

[11] Y. Wang, J. Bokor, and A. Lee, "Maskless lithography using drop-on-demand inkjet printing method," vol. 5374, pp. 628–636, 2004.

[12] *Fundamentals of Heat and Mass Transfer*. Pearson Education, 2009.

[13] Y. H. Jo, I. Jung, C. S. Choi, I. Kim, and H. M. Lee, "Synthesis and characterization of low temperature sn nanoparticles for the fabrication of highly conductive ink," *Nanotechnology*, vol. 22, no. 22, p. 225701, 2011.

[14] A. L. Efros and B. I. Shklovskii, "Critical behaviour of conductivity and dielectric constant near the metal-non-metal transition threshold," *physica status solidi (b)*, vol. 76, no. 2, pp. 475–485, 1976.

[15] S. Beglio, G. Muscato, N. Pitrone, and N. Savalli, "Automatic measurement system for the estimation of surface resistivity distribution," in *Instrumentation and Measurement Technology Conference, 2001. IMTC 2001. Proceedings of the 18th IEEE*, vol. 2, 2001, pp. 902–905 vol.2.

[16] P. Pesikan, M. Joy, G. Scott, and R. Henkelman, "Two-dimensional current density imaging," *Instrumentation and Measurement, IEEE Transactions on*, vol. 39, no. 6, pp. 1048–1053, Dec 1990.

[17] J. Jackson, *Classical Electrodynamics*. Wiley, 1998.

[18] P. Hölzl and B. Zagar, "Deconvolution of high-resolution magnetic field scans for improved current density imaging," *IEEE Transactions on Magnetics*, vol. 50, no. 2, pp. 101–104, February 2014.